ELSEVIER SCIENTIFIC PUBLISHERS IRELAND

Cancer Letters 77 (1994) 163–171

CANCER LETTERS

Machine learning techniques to diagnose breast cancer from image-processed nuclear features of fine needle aspirates

William H. Wolberg*[a], W. Nick Street[b], O.L. Mangasarian[b]

[a]*Departments of Surgery and Human Oncology, University of Wisconsin, Madison, WI 53792, USA*
[b]*Computer Sciences Department, University of Wisconsin, Madison, WI 53706, USA*

(Received 9 September 1993; revision received 28 November 1993; accepted 28 September 1993)

Abstract

An interactive computer system evaluates and diagnoses based on cytologic features derived directly from a digital scan of fine-needle aspirate (FNA) slides. A consecutive series of 569 patients provided the data to develop the system and an additional 54 consecutive, new patients provided samples to test the system. The projected prospective accuracy of the system estimated by tenfold cross validation was 97%. The actual accuracy on 54 new samples (36 benign, 1 atypia, and 17 malignant) was 100%. Digital image analysis coupled with machine learning techniques will improve diagnostic accuracy of breast fine needle aspirates.

Key words: Breast cancer; Digital morphometry; Image analysis; Machine learning; Fine needle aspiration

1. Introduction

The accuracy of visually diagnosed breast fine needle aspirates (FNA) is over 90%. The overall accuracy was 94.3% in a 37-series study reported by Frable [8] plus 25 more recent series [1,3,4, 6,7,10–14,18–20,25–27,30,32–35,38–40], with a total of 23 741 satisfactory breast FNAs. Individually, the mean sensitivity for these series was 0.91 ± 0.07 and the mean specificity was 0.87 ± 0.18. The relatively high standard deviations indicate that the accuracy achieved in individual series varies considerably and reflects the subjectivity of visual diagnosis. Additionally, publication bias is toward placing favorable results in the literature. Giard and Hermans [9] emphasized the need for developing individual performance characteristics for persons doing this test. The subjectivity which is inherent in visual diagnosis can be minimized with computer-based digital image analysis and machine learning techniques [37]. This technology will enhance the usefulness of fine needle aspiration as a diagnostic tool for breast cancer.

2. Patients and methods

A consecutive series of 569 patients (212 cancer and 357 benign) provided the data for the study. An additional 54 consecutive, new patients provided samples to test the system. All cancers and some of the benign masses were histologically confirmed. The remaining benign masses were followed for a year and were biopsied if they changed in size

* Corresponding author.

0304-3835/94/$06.00
SSDI 0304-3835(94)03273-L

or character. Cancer patients were given standard surgical and chemotherapy treatment. Adjunctive radiotherapy was given when indicated.

2.1. Fine needle aspiration

A small drop of viscous fluid was aspirated from breast masses by making multiple passes with a 23-gauge needle as negative pressure was applied to an attached syringe. The aspirated material was expressed onto a silane-coated glass slide. A similar slide was placed face down on the aspirate, and the aspirate was spread as the slides were separated with a horizontal motion. Preparations were immediately fixed in 95% ethanol and examined after they were stained with hematoxylin and eosin. Only palpable masses were aspirated and only solid masses which yielded epithelial cells were analyzed.

3. Nuclear feature characterization

3.1. Image preparation

The area on the aspirate slides to be analyzed was visually selected for minimal nuclear overlap. Areas of apocrine metaplasia were avoided. The image for digital analysis was generated by a JVC TK-1070U color video camera mounted above an Olympus microscope and the image was projected into the camera with a 63× objective and a 2.5× ocular. The image was captured by a ComputerEyes/RT color framegrabber board (Digital Vision, Inc., Dedham MA) as a 512 × 480, 8 bit/pixel Targa file.

3.2. The digital assessment process

The first step in successfully analyzing the digital image was to specify the exact location of each cell nucleus. A graphical user interface was developed that allows the user to input the approximate location of sufficient nuclei to provide a representative sample. The interface was developed using the X Window System and the Athena WidgetSet on a DECstation 3100. A mouse button was used to trace a rough outline of each visible cell nucleus.

3.3. Snakes

Beginning with a user-defined approximate border as an initialization, the actual cell nuclear boundary was located by an active contour model known in the literature as a 'snake' [17,42]. A snake is a deformable spline which seeks to minimize an energy function defined over the arclength of a curve. We define the energy function in such a way that the snake, in the form of a closed curve, conforms itself to the boundary of a cell nucleus. To achieve this, the energy function to be minimized is defined as the following function of arclength:

$$E = \int_s (\alpha E_{\text{cont}}(s) + \beta E_{\text{curv}}(s) + \gamma E_{\text{image}}(s))ds$$

Here E represents the total energy integrated along the arclength s of the snake. The energy computation is the integral of energy terms E_{cont}, E_{curv} and E_{image}, with respective weights α, β, and γ controlling their relative importance. To avoid performing the necessary variational calculus, the energy function is computed at a number of discrete points along the curve, and the integral is approximated with a sum. The three energy terms measure the following quantities.

E_{cont}: this term is constructed to penalise discontinuities in the curve. In the discrete case, this term measures how evenly spaced the snake points are. This counteracts the tendency of the snake points to cluster near regions of sharp gray scale discontinuities. The distance from a snake point to one of its neighbors is found and compared to the average distance between adjacent points. The magnitude of this difference is then E_{cont}.

E_{curv}: this geometric term measures discontinuities in the curvature of the snake. Cell nuclei are more or less ellipsoidal; the curvature of the nuclear boundary should be approximately the inverse of the radius, and should change slowly from one part of the boundary to another. Hence, points with abnormally high curvature (sharp corners) or low curvature (straight line segments) are penalized. This term allows the snake to take on a reasonable shape even in regions where gray scale information is lacking, for instance, where cells overlap. The distance from a snake point to the center (i.e., length of radial line) is then compared to the average of such distances in a neighborhood

of the point. The magnitude of the difference is this energy term E_{curv}.

E_{image}: this term ties the snake's performance to the underlying image. In our case E_{image} measures the gray-level contrast between pixels inside the snake and those outside the snake. Taking advantage of the fact that cell nuclei are generally darker than the surrounding material, we define this term such that lowest energy is achieved by a sharp, dark-to-light transition. Hence, an edge detection template is rotated so the expected edge is perpendicular to the radial line of the nucleus at that point. For instance, the following edge template would be applied for a snake point directly above the center of the nucleus:

1	2	1
0	0	0
−1	−2	−1

Thus, gray scale discontinuities which are perpendicular to the radial line produce the highest edge score. E_{image} is defined so a sharp discontinuity minimizes the energy value. Since light intensity is the most important factor in finding the nuclear boundary, this term is weighted somewhat more heavily than the other two, i.e. $\gamma > \alpha$ and $\gamma > \beta$.

The optimal local value of the energy function is approximated using an algorithm due to Williams and Shah [42]. If the function value at a particular snake point can be lowered by moving the point to an adjacent pixel, then it is moved, thus possibly affecting the energy computation at other points. The process is repeated for each point, in turn, until all points settle into a local minimum of the energy function. Since a local or greedy convergence algorithm is used, the snake may converge to a local energy minimum that is a poor representation of the cell nucleus boundary. In this case, the user can use the mouse pointer to delete the snake and initialize a new one in its place. Most of the snakes perform quite well, conforming closely to the nuclear boundaries very quickly.

3.4. Nuclear features

An area on the cytology slide was visually selected for optimal digital analysis and one image was made of this area. The area selected contained the most abnormal appearing cells in which monolayered nuclei were present. By using the computer-generated snakes, ten nuclear features were calculated for each cell. These features are modeled such that higher values are typically associated with malignancy. The mean value, worst (mean of the three largest values), and standard error of each feature were computed for each image, resulting in a total of 30 features for each case in the study.

3.5. Radius

The radius of an individual nucleus is measured by averaging the length of the radial line segments defined by the centroid of the snake and the individual snake points.

3.6. Perimeter

The total distance between consecutive snake points constitutes the nuclear perimeter.

3.7. Area

Nuclear area is measured simply by counting the number of pixels on the interior of the snake and adding one-half of the pixels on the perimeter.

3.8. Compactness

Perimeter and area are combined [2] to give a measure of the compactness of the cell nuclei using the formula perimeter^2/area. This dimensionless number is at a minimum with a circular disk and increases with the irregularity of the boundary. However, this measure of shape also increases for elongated cell nuclei, which do not necessarily indicate an increased likelihood of malignancy. The feature is also biased upward for small cells because of the decreased accuracy imposed by digitization of the sample.

3.9. Smoothness

The smoothness of a nuclear contour is quan-

tified by measuring the difference between the length of a radial line and the mean length of the lines surrounding it. This is similar to the curvature energy computation in the snakes.

3.10. Concavity

In a further attempt to capture shape information we measure the number and severity of concavities or indentations in a cell nucleus. We draw chords between non-adjacent snake points and measure the extent to which the actual boundary of the nucleus lies on the inside of each chord. This feature is greatly affected by the length of these chords, as smaller chords better capture small concavities. We have chosen to emphasize small indentations, as larger shape irregularities are captured by other features.

3.11. Concave points

This feature is similar to concavity but measures only the number, rather than the magnitude, of contour concavities.

3.12. Symmetry

In order to measure symmetry, the major axis, or longest chord through the center, is found. We then measure the length difference between lines perpendicular to the major axis to the nuclear boundary in both directions. Special care is taken to account for cases where the major axis cuts the boundary because of a concavity.

3.13. Fractal dimension

The fractal dimension of a nuclear boundary is approximated using the 'coastline approximation' described by Mandelbrot [21]. The perimeter of the nucleus is measured using increasingly larger 'rulers'. As the ruler size increases, decreasing the precision of the measurement, the observed perimeter decreases. Plotting log of observed perimeter against log of ruler size and measuring the downward slope gives (the negative of) an approximation to the fractal dimension. As with all the shape features, a higher value corresponds to a less regular contour and thus to a higher probability of malignancy.

3.14. Texture

The texture of the cell nucleus is measured by finding the variance of the gray scale intensities in the component pixels.

4. Phantoms

A series of four shapes (round, ellipse, moon, and rough) in three sizes were generated in order to compare digital feature assessments with visual characteristics (Fig. 1). The results are shown in Table 1. Size is measured by radius and area. Shape is measured by smoothness, concavity, compactness, concave points, symmetry and fractal dimension. Although initially thought to measure size, the measurement of the phantoms

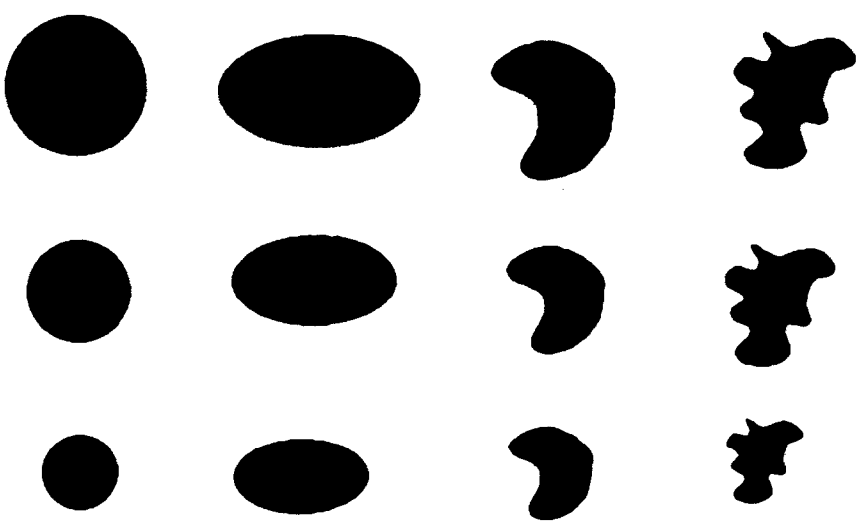

Fig. 1. 'Nuclear features' of four shapes and three sizes (phantoms) were digitally analyzed.

Table 1
Normalized measurement of digital features on phantoms

		Radius	Perimeter	Smoothness	Concavity	Symmetry	Area	Compactness	Concave points	Fractal dimension
Circle	Large	0.96	0.67	0.39	0.06	0.23	0.94	0.01	0.13	0.18
	Medium	0.83	0.57	0.39	0.06	0.20	0.67	0.02	0.07	0.19
	Small	0.62	0.41	0.31	0.01	0.25	0.36	0.00	0.02	0.20
Ellipse	Large	1.00	0.74	0.48	0.11	0.35	0.97	0.13	0.34	0.30
	Medium	0.85	0.61	0.40	0.08	0.61	0.66	0.13	0.24	0.33
	Small	0.63	0.46	0.57	0.06	0.37	0.38	0.14	0.20	0.38
Moon	Large	0.99	0.83	0.60	0.23	0.90	1.00	0.33	0.61	0.49
	Medium	0.86	0.71	0.44	0.23	1.00	0.73	0.34	0.44	0.50
	Small	0.65	0.52	0.47	0.25	0.99	0.40	0.32	0.39	0.50
Rough	Large	0.95	1.00	0.81	0.79	0.99	0.90	1.00	0.97	1.00
	Medium	0.83	0.85	0.89	0.81	0.91	0.68	0.91	0.94	0.95
	Small	0.63	0.62	1.00	1.00	0.89	0.38	0.86	1.00	0.99

determined that both size and shape are measured by perimeter (Fig. 1). Each phantom was measured three times and the mean values and standard error of each feature were calculated for each phantom.

4.1. Classification procedure

Image processing produces a database of one point with 30 dimensions for each sample. The classification procedure becomes one of pattern separation, specifically, that of determining how points can best be separated into benign and malignant sets. The classification procedure is a variant on the multisurface method (MSM) [22,24] known as MSM-Tree (MSM-T) [5,23]. This method uses linear programming iteratively to place a series of separating planes in the feature space of the examples. If the two sets can be separated by a single plane, the first plane will be so placed between them. If the sets are not linearly separable, MSM-T constructs a plane that minimizes an average distance of misclassified points. The procedure is recursively repeated on the two regions generated by each plane until each of the final regions contains mostly points of one category. The classifier thus obtained is then used to categorize new cases. In order to generate a classifier that generalizes well to unseen cases, we sought to minimize not only the number of separating planes but also the number of features used. As a rule, simpler classifiers perform better than more complex ones on new data. The best single-plane classifier separated benign from malignant points based on three nuclear feature values for each case: mean texture, the worst area, and the worst smoothness. With a single plane classifier, the probability of a specific sample being malignant can be estimated. This information is shared with the patient and the decision whether to follow or to biopsy an apparently benign mass is made.

Distribution curves for malignant and benign points are determined by projecting the positions which the malignant and benign points occupy in three dimensional space (determined by the values for mean texture, worst area and worst smoothness) onto the normal line of the separating plane. The estimated probability of malignancy for a new point is determined from the ratio of the intercepts at that point with the malignant and benign distribution curves as determined by Parzen windows technique [28] (Figs. 2–4).

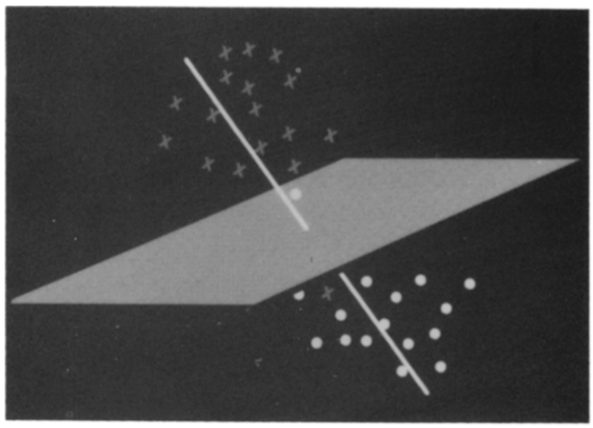

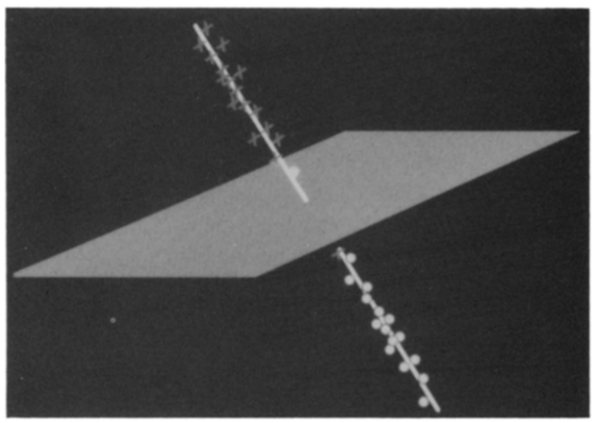

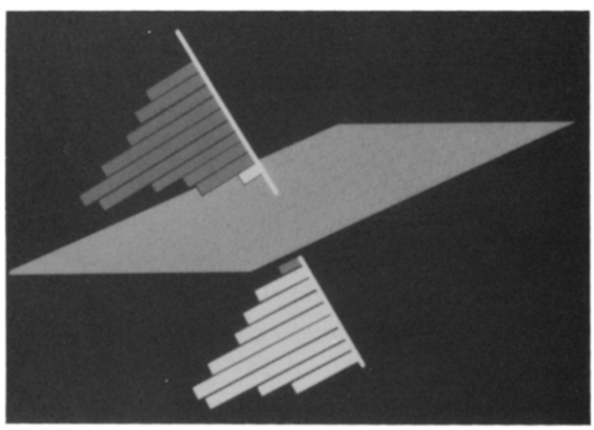

Figs. 2–4. Graphic representation of the separating plane between two categories of points and the normal line of the separating plane. The actual position which the points occupy in three dimensional space is represented in Fig. 2. The projection of these points onto the normal line of the separating plane is represented in Fig. 3. The histogram of the distribution of the points is depicted in Fig. 4. This is the reference for determining the estimated probability of malignancy of a new point.

4.2. Estimate of predictive accuracy

A tenfold cross-validation [36] was performed in order to estimate diagnostic predictive accuracy. This train-and-test procedure divides the data set into ten randomly selected, equally sized parts and uses each in turn as a test set on a classifier created from the remaining nine sets. This estimate is unbiased and also very accurate in cases such as ours which have a fairly large number of training samples. The accuracy was directly tested by the analysis of 54 newly obtained samples (36 benign, 1 atypia and 17 malignant).

5. Results

5.1. Diagnostic separation

The best single-plane diagnostic classifier based on mean texture, the worst area, and the worst smoothness separated 97.3% of the cases successfully. The projected prospective accuracy was 97%. Using the standard error from the binomial distribution [41], we can be confident at the 95% level that the true prospective accuracy lies between 95.5% and 98.5%. Fifty-four (17 malignant, 36 benign, and 1 papilloma with atypia) samples which were obtained subsequent to the development of the trained diagnostic algorithm were used to test its accuracy. The machine diagnosis was correct in all instances. The machine diagnosis was ambiguous in the case of the papilloma with atypia. The machine diagnosis based on the MSM-T plane was benign, but the estimated probability

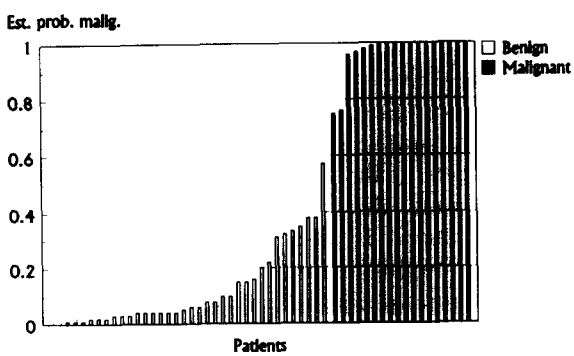

Fig. 5. The estimated probability of malignancy for 54 new samples as diagnosed by the trained algorithm together with their actual diagnoses.

of malignancy based on the distribution curves was 0.57. The estimated probability of malignancy for all the 54 new samples and their actual diagnoses is shown in Fig. 5.

6. Discussion

Other researchers have applied computer based image analysis to various aspects of breast cytology interpretation. Wittekind and Schulte [43] found that mean nuclear area, mean maximum nuclear diameter and mean nuclear perimeter differed significantly between benign and malignant breast cell obtained by FNA. Additionally, they showed that computer-assisted image analysis was superior to eyepiece measurement with respect to accuracy and reproducibility of the results. Other studies either have used direct scanning of Feulgen stained material [29] or have analyzed digitized images as we have done [16,31,43]. Direct scanning techniques generally analyze only size and texture features whereas analysis of digitized images also allows measurement of shape features. Those who have analyzed digitized images obtained them by manually tracing the nuclear outline on a digitizing tablet. In contrast, we used a 'mouse' to manually outline the digitized nucleus on a computer monitor and relied on our snake program to conform the rough outline to the actual nuclear boundary. The snake program accomplishes segmentation but other image processing methods may also be appropriate (e.g. region growing).

Hutchinson et al. analyzed clump characteristics in breast aspirates but found them to add little to diagnostic accuracy [15]. Their diagnostic accuracy using only cell features was 83.6%, using only smear characteristics was 70.5%, and using both was 86.9%. We achieved better accuracy using only cell features. The analytical methods which we used to project prospective accuracy are familiar to the machine learning community but have been under-utilized in the medical community.

Our computerized system is intended to address the case of multiple and possibly less experienced observers. Still, computerization of cytological analysis as described here requires some degree of operator input. Intra- and interobserver reproducibility of our system was determined to be satisfactory despite intentional testing with untrained observers [44]. A minimal training session, coupled with the increased accuracy of computerized image processing and the robustness of a good machine learning procedure, should reduce or even eliminate the interobserver variability inherent to visual interpretation.

We plan to adapt our UNIX-based system for a portable DOS based application. Use of the system will require a video camera attachment for a microscope, a frame grabber board and the appropriate expert system software. Two alternatives exist for the expert system software. Either an individual expert system can be generated by the user from one's own cytology collection, or the FNA slides can be prepared in the manner described herein and our expert system based on 569 samples can be used and expanded. These techniques estimate the probability of malignancy in borderline cases and decisions for open biopsy can be objectively made. The present work is a step toward increasing the diagnostic usefulness of fine needle aspiration biopsy.

7. Acknowledgements

This study was supported in part by Air Force Office of Scientific Research grant AFOSR 89-0410 and National Science Foundation grant CCR-9101801.

8. References

1 Abele, J.S., Miller, T.R., Goodson, W.H.I and Hohn, D.C. (1983) Fine-needle aspiration of palpable breast masses. A program for staged implementation. Arch. Surg., 118, 859–863.

2 Ballard, D. and Brown, C. (1982) Computer Vision. Prentice-Hall, Inc., Englewood Cliffs, New Jersey.

3 Barrows, G.H., Anderson, T.J., Lamb, J.L. and Dixon, J.M. (1986) Fine-needle aspiration of breast cancer. Relationship of clinical factors to cytology results in 689 primary malignancies. Cancer, 58, 1493–1498.

4 Bell, D.A., Hajdu, S.I., Urban, J.A. and Gaston, J.P. (1983) Role of aspiration cytology in the diagnosis and management of mammary lesions in office practice. Cancer, 51, 1182–1189.

5 Bennett, K.P. (1992) Decision Tree Construction via Lin-

ear Programming. In: Proceedings of the 4th Midwest Artificial Intelligence and Cognitive Science Society Conference, pp. 97–101. Editor: M. Evans. (Also available on request as Technical Report No. 1067, Computer Sciences Dept., University of Wisconsin, 1210 W. Dayton St., Madison, WI 53706).

6 Bjurstam, N., Hedberg, K., Hultborn, K.A., Johansson, N.T. and Johnsen, C. (1974) Diagnosis of breast carcinoma: Evaluation of clinical examination, mammography, thermography and aspiration biopsy in breast disease. Progr. Surg., 13, 1–65.

7 de Ranieri, E., Mandard, A.M., Juret, P., Couette, J.E., Delozier, T. and Ollivier, J.M.L.G. (1983) Fiabilite de la ponction cytologique. Qui foit ponctionnner les tumeurs du sein? La Presse Med., 12, 1527–1529.

8 Frable, W.J. (1983) Thin-needle aspiration biopsy. Major Problems in Pathology. WB Saunders Co., Philadelphia.

9 Giard, R.W.M. and Hermans, J. (1992) The value of aspiration cytologic examination of the breast. A statistical review of the medical literature. Cancer, 69, 2104–2110.

10 Griffith, C.N., Kern, W.H. and Mikkelsen, W.P. (1986) Needle aspiration cytologic examination in the management of suspicious lesions of the breast. Surg. Gynecol. Obstet., 162, 142–144.

11 Gupta, R.K., Dowle, C.S. and Simpson, J.S. (1990) The value of needle aspiration cytology of the breast, with an emphasis on the diagnosis of breast disease in young women below the age of 30. Acta Cytol., 34, 165–168.

12 Halevy, A., Reif, R., Bogolovsky, H. and Orda, R. (1987) Diagnosis of carcinoma of the breast by fine needle aspiration cytology. Surg. Gynecol. Obstet., 164, 506–508.

13 Hammond, S., Keyhani-Rofagha, S. and O'Toole, R.V. (1987) Statistical analysis of fine needle aspiration cytology of the breast. Acta Cytol., 31, 276–280.

14 Horgan, P.G., Waldron, D., Mooney, E., O'Brien, D., McGuire, M. and Given, H.F. (1991) The role of aspiration cytologic examination in the diagnosis of carcinoma of the breast. Surg. Gynecol. Obstet., 172, 290–292.

15 Hutchinson, M.L., Isenstein, L.M. and Zahniser, D.J. (1991) High-resolution and contextual analysis for the diagnosis of fine needle aspirates of breast. Anal. Quant. Cytol. Histol., 13, 351–355.

16 Hutchinson, W.B., Thomas, D.B., Hamilin, W.B., Roth, G.F. and Peterson, A.V. (1980) Risk of breast cancer in women with benign breast disease. J. Natl. Cancer Inst., 65, 13–20.

17 Kass, M., Witkin, A. and Terzopoulos, D. (1987) Snakes: Active contour models. Proc. First Int. Conf. Comput. Vision, 259–269.

18 Kline, T. (1981) Handbook of Fine Needle Aspiration Biopsy Cytology. C.V. Mosby, Saint Louis, MO.

19 Knight, C.D.J, Ingle, J.N., Gaffey, T.A. et al. (1986) Surgical considerations after chemotherapy and radiation therapy for inflammatory breast cancer. Surgery, 99, 385–391.

20 Koivuniemi, A.P. (1976) Fine-needle aspiration biopsy of the breast. Ann. Clin. Res., 8, 272–283.

21 Mandelbrot, B.B (1977) The Fractal Geometry of Nature. W.H.Freeman and Company, New York, NY.

22 Mangasarian, O.L. (1968) Multi-surface method of pattern separation. IEEE Trans Inf. Theory, IT-14, 801–807.

23 Mangasarian, O.L. (1992) Mathematical programming in neural networks. Technical Report No. 1129, Computer Sciences, Univ Wisc. (Available on request, Computer Sciences Dept., University of Wisconsin, 1210 W. Dayton St., Madison, WI 53706).

24 Mangasarian, O.L., Setiono, R. and Wolberg, W.H. (1990) Pattern recognition via linear programming: Theory and application to medical diagnosis. In: Large-Scale Numerical Optimization, pp. 22–30. Editors: T.F. Coleman and Y. Li. SIAM, Philadelphia, PA.

25 Nicholson, S., Sainsbury, J.R.C., Wadehra, V., Needham, G.K. and Farndon, J.R. (1988) Use of fine needle aspiration cytology with immediate reporting in the diagnosis of breast disease. Br. J. Surg., 75, 847–850.

26 Painter, R.W. and Clark, W.E.I (1988) Negative findings on fine-needle aspiration biopsy of solid breast masses: Patient management. Am. J. Surg., 155, 387–390.

27 Palombini, L., Fulciniti, F., Vetrani, A., De Rosa, G., Di Benedetto, G., Zeppa, P. and Troncone, G. (1988) Fine-needle aspiration biopsies of breast masses. A critical analysis of 1956 cases in 8 years (1976–1984). Cancer, 61, 2273–2277.

28 Parzen, E. (1962) On estimation of a probability density and mode. Ann. Math. Stat., 35, 1065–1076.

29 Pienta, K.J. and Coffey, D.S. (1991) Correlation of nuclear morphometry with progression of breast cancer. Cancer, 68, 2012–2016.

30 Pilotti, S., Rilke, F., Delpiano, C., Di Pietro, S. and Guzzon, A. (1982) Problems in fine-needle aspiration biopsy cytology of clinically or mammographically uncertain breast tumors. Tumor, 68, 407–412.

31 Salmon, I., Coibion, M., Larsimont, D., Badr-El-Din, V. et al. (1991) Comparison of fine needle aspirates of breast cancers to imprint smears by means of digital cell image analysis. Anal. Quant. Cytol. Histol., 13, 193–200.

32 Schondorf, H. and Schneider, V. (1978) Aspiration Cytology of the Breast. WB Saunders Co., Philadelphia.

33 Smallwood, J., Herbert, A., Guyer, P. and Taylor, I. (1985) Accuracy of aspiration cytology in the diagnosis of breast disease. Br. J. Surg., 72, 841–843.

34 Smith, C., Butler, J., Cobb, C. and State, D. (1988) Fine-needle aspiration cytology in the diagnosis of primary breast cancer. Surgery, 103, 178–183.

35 Somers, R.G., Young, G.P., Kaplan, M.J., Bernhard, V.M., Rosenberg, M. and Somers, D. (1985) Fine-needle aspiration biopsy in the management of solid breast tumors. Arch. Surg., 120, 673–677.

36 Stone, M. (1974) Cross-validatory choice and assessment of statistical predictions. J. R. Stat. Soc., 36, 111–147.

37 Street, W.N., Wolberg, W.H. and Mangasarian, O.L. (1993) Nuclear feature extraction for breast tumor diag-

nosis. Proc. IS&T/SPIE Int. Symp. Electron. Imaging, 1905, 861–870.

38 Ulanow, R.M., Galblum, L. and Canter, J.W. (1984) Fine needle aspiration in the diagnosis and management of solid breast lesions. Am. J. Surg., 148, 653–657.

39 Vetrani, A., Fulciniti, F., de Benedetto, G., Zeppa, P., Troncone, G. and et al., (1992) Fine-needle aspiration biopsies of breast masses. An additional experience with 1153 cases (1985 to 1988) and a meta-analysis. Cancer, 69, 736–740.

40 Wanebo, H.J., Feldman, P.S., Wilhelm, M.C., Cocell, F.L. and Binns, R.L. (1984) Fine needle aspiration cytology in lieu of open biopsy in management of primary breast cancer. Ann. Surg., 199, 569–579.

41 Weiss, S. and Kulikowski, C.A. (1991) Computer Systems That Learn, Morgan Kaufmann, San Mateo, CA.

42 Williams, D.J. and Shah, M. (1990), A fast algorithm for active contours. In: Proc. Third Int. Conf. Computer Vision, pp. 592–595. Osaka, Japan.

43 Wittekind, C. and Schulte, E. (1987) Computerized morphometric image analysis of cytologic nuclear parameters in breast cancer. Anal. Quant. Cytol. Histol., 9, 480–484.

44 Wolberg, W.H., Street, W.N. and Mangasarian, O.L. (1993) Breast cytology diagnosis via digital image analysis. Anal. Quant. Cytol. Histol. (in press).